Rock Mechanics and Rock Engineering (2022) 55:2879–2898
https://doi.org/10.1007/s00603-021-02619-4

ORIGINAL PAPER

Exploring the Deformation Mechanics of Coal Ribs Using the Distinct Element Modeling Approach

Maurice Sunkpal[1] · **Taghi Sherizadeh**[1]

Received: 31 December 2020 / Accepted: 12 August 2021 / Published online: 21 August 2021

Abstract

Understanding coal rib geomechanics is essential for improving rib stability and eliminating fatality and injury trends due to rib failures. There are presently no standardized rib control practices available in most countries. In light of this observed dearth, this investigation aims to improve understanding of rib failure mechanisms using the distinct element modeling (DEM) technique. DEM is chosen because of its superior advantage to explicitly represent discontinuities and their constitutive behaviors, besides that of the intact rock matrix. To analyze the rib stability, a numerical monitoring protocol is implemented to monitor the deformation characteristics of the coal rock mass as its strength is gradually reduced and the deformation and safety factors are established. A number of scenarios were considered in the modeling process, including a non-cleated rib, a cleated rib, and the interaction between support and coal mass. The main conclusions drawn from the study were that the rib failure process initiated with tensile and shear cracks which coalesced to form predominantly sub-parallel tensile fractures to the rib line; and joints and defects in the rib limit fracture development and propagation. The depth of fracture was found to be ~ 1.14 m for the cleated rib and ~ 1.40 m for the non-cleated rib. The depth of softening (DOS) for the cleated and non-cleated ribs was ~ 1.80 m and ~ 1.60 m, respectively. Also, the results demonstrated the capability of DEM-based bonded block models (BBM) in explicitly capturing the rock and support interactions which makes this solution to be suitable for investigating coal rib stability and support requirements.

Keywords Coal rib geomechanics · Depth of softening · Distinct element modeling · Coal rib stability · Assessing support requirement

1 Introduction

Fatalities and injuries resulting from rib failures in the coal mining industry have propelled the research of coal rib stability to the forefront of ground control efforts. This surge in research is geared toward understanding the mechanisms driving rib instability (Mohamed et al. 2016, 2020a, 2020b; Rashed et al. 2021). Understanding coal rib geomechanics is essential for stability control purposes. This knowledge is also vital in determining support requirements. The rib control practices currently being used have their origins traceable to roof control techniques. This is because compared to coal rib, coal roof has received tremendous research and enough knowledge gained about their performance. It is true that there is inadequate knowledge and understanding of the geomechanical behavior of ribs. Data from the Mine Safety and Health Administration (MSHA) has attributed more than half of ground fall fatalities in the recent decade to rib failures in underground coal mines in the United States (MSHA 2018).

Several parameters have been identified as capable of providing useful information on the performance of coal pillar ribs. These are categorized into the following: rib support load measurement, vertical rock stress distribution, and horizontal rib displacement (Bigby and Cassie 2003). There is considerable work on the distribution of vertical stresses on the mine rib side. A major proportion of this is focused on pillar design. Wilson (1983) propounded the theory of the *yield zone,* recognizing that yield zones develop around excavations and that these cause excavation to close. The theory has become the basis for analyzing the behavior of soft rocks in deep mining excavations. The observed mechanical behavior of coal formations around openings

✉ Taghi Sherizadeh
sherizadeh@mst.edu

[1] Missouri University of Science and Technology, Rolla, MO, USA

makes this theory particularly relevant for coal rib analysis. Kirsch's (1898) linear elastic theory predicts high tangential stresses around the boundaries of excavations. This usually results in a high concentration of vertical stresses around mine rib sides. In-situ vertical stress is proportional to the depth of the excavation. Thus, vertical stress concentration at the coal rib will increase with depth. Therefore, as the excavation starts to develop in the coal body, the vertical stress concentration at the rib side increases in a greater proportion exceeding the strength of the coal. The rib therefore yields or softens in response to the increased stress extending some distance into the rib. At a certain level of confinement defined by the frictional characteristics of the coal and the frictional contacts of the surrounding rock, the rock strength will exceed the vertical stress concentration. Under these conditions, the depth of the yield zone will be established. This stage will also define the occurrence of the peak vertical stress in the rib. Beyond the yield zone, the rock remains intact, and the vertical stress will gradually reduce until it equates with the overburden load. At this point, the mode of failure in the rib is dependent on the post-failure characteristics of the rib and the local stiffness of the mining system (Salamon 1970, 1974).

Besides vertical stresses driving rib compressive failures, there is also the mechanism of shear deformation, which, like the compressive failures, result from a relatively high-stress regime. Shear planes develop within the roof, which extends up into the roof and down into the floor. This typically causes the coal ribline at the base of the rib to bulge into the excavation, accompanied by floor heave, as the coal rib rotates about the shear surface within the ribline. There is also a slabbing failure, which occurs when the rib sides lean into the roadway because of significant decoupling at or near roof level. Slabs of the material may become free, especially where there is a pervasive coal cleat orientated unfavorably to the roadway drivage direction. The floor heave usually holds the base of the rib in place in this scenario. Toppling failure of the upper ribside can also occur when the lower rib becomes degraded, leading to the upper rib overhanging. These rib deformation mechanisms are not exclusive, and a combination of these can occur at any mine site. Another category of rib failure, aside the stress related ones discussed, are the types driven by kinematic failure. These failure modes include wedge, toppling and planar. They are usually caused by the presence of a discontinuity, fracture, joint or cleat, to create a plane to facilitate the kinematic failure mechanism (Heritage 2019). These factors are interrelated, and a combination of these factors usually affects the rib performance.

The deformation of the rock mass surrounding the excavation is a primary concern for ground control engineers. It is also the fundamental reason that guides the installation of reinforcement. Rock mass deformation is also the single most significant physical quantity by which numerical modeling and back analysis results can be verified (Sakurai et al. 2003; Li et al. 2005; Zhu et al. 2008b). Two methods are often employed to measure deformation in the rock mass surrounding an excavation: (a) convergence measurement done at the rib line and (b) displacement measurement in the surrounding rock masses (Zhu et al. 2010). Monitoring studies are often used in practice to investigate the integrity and stability of rock structures in rock engineering projects. These often range from crude methods such as a prop and tape to highly sophisticated extensometers. Several studies have described the application of extensometers for deformation measurement and coal pillar performance appraisal (British Coal 1990, 1992, 1993; Hebblewhite et al. 1998; Colwell and Mark 2005; Heritage 2019). Lateral rib displacement monitoring is important for rib control purposes since it directly translates into the expected movement mine personnel attempts to control (Sears et al. 2018). Data from these monitoring schemes often serve the important purpose of providing insight for decision-making with regards to the adequacy of support, rib performance, and its associated deformation mechanics.

Another criterion often considered by engineers in deciding the competence of a rock structure to perform its design objectives is the factor of safety (FS) analysis. The FS is used to provide for the uncertainties associated with any design, particularly during preliminary design studies, when the amount of information available is limited. There are no hard and fast rules to select a target FS. The fundamental consideration is the consequences of failure. In addition, some important considerations should include: (1) variations in rock mass properties and in the performance of the rock structure; (2) scale dependency of rock mass strength; (3) type of loading (static, dynamic, etc.); (4) effect of stress concentrations, residual stress, etc.; and (5) overall concern of human safety. Caution should be placed on the application of FS as improper use of it usually results in an inefficient design that can result in waste or catastrophic failure. There are several definitions in use for FS, but most of them belong to one of the two principle definitions: (1) The practical definition is stated as for a given strength of a structure, the FS of the system can be determined for an applied stress state as the ratio of the strength to the applied stress; (2) The numerical approach which is based on the strength reduction method (SRM) is defined as the ratio of the actual or designed strength to the strength parameter that activates failure. A good amount of information on the SRM method can be found in Diederichs et al. (2007a). Mohamed et al. (2019) presented a good review of some of the most commonly used calculation methods for FS using SRM. The FS of coal mine pillar is commonly determined using empirical formulas. There are some notable limitations of this approach as summarized in (Frith and Reed 2019):

The pillar strength formulae derived by Salamon and Munro (1967) are based on the condition that the width of a panel of pillars had to be at least equal to the depth of mining. The assumption was that this will result in full tributary loading. According to Galvin (2006), there are some mining environments in which mining span must exceed depth by a considerable margin to achieve full deadweight loading; these methods include room-and-pillar-mining and longwall mining. These are the dominant coal mining methods in the USA. Hence, it is logical to conclude that these data points may have contributed to pillar strength being overestimated by Salamon and Munro (1967). Normally, this should be of no consequence because it is reflected in the probability of design success associated with any given safety factor (Galvin 2006). Additionally, empirical methods, which are mostly based on the analysis of case histories, have found wide acceptance as a tool for engineering design. This makes them limited in application to cases beyond the limits of the case histories from which they were developed (Esterhuizen 2014). Also noted by Galvin (2016) is the mixed success experience by the field application of these methods. Besides the aforementioned shortfalls of the empirical methods, these methods do not consider the interrelationship between stress, strength, and displacement (Krahn 2003). Not considering the interaction between displacements and stresses, the post-failure behavior emphasizes the assumption that strength is independent of deformation, thus a perfectly plastic behavior.

The rib control practices currently being used have their origins traceable to roof control techniques. This is because compared to coal rib, coal roof has received tremendous research and enough knowledge gained about their performance. Understandably, applying roof control methods to coal rib is guaranteed to cause rib stability problems. The structural layout of the geological units, such as bedding planes, cleats, partings, etc., in the roof and rib with respect to the excavation face is different. The presence of these geologic units and their characteristics have an important influence on the stability of coal ribs. It is true that there is inadequate knowledge and understanding of the geomechanical behavior of ribs. In light of this observed dearth, this investigation aims to contribute to the knowledge of rib behavior using the distinct element modeling (DEM) technique to explore the deformation and loading behaviors of coal ribs. DEM is chosen because of its superior advantage to explicitly represent both discontinuities and their constitutive behaviors, besides that of the intact rock matrix.

This paper uses the bonded block model (BBM) approach, implemented in the universal distinct element code, UDEC (Itasca 2019), to analyze the stability of a typical coal pillar rib. The BBM can model intact or a rock mass as bonded polygonal elements. The BBM method, which is a discontinuum DEM approach, simulates the initiation of cracks that can coalesce and/or propagate leading to extension and shear fracturing, as well as the rock (e.g., intact, jointed, or veined) strength dependency on confinement. Studies prior have validated this method as efficient and compatible with engineering practices and capable of representing the overall behavior of the rock mass [Coggan et al. 2012; Gao and Stead 2014; Gao et al. 2014 (Triangular blocks); Zhu et al. 2017; Zhu et al. 2020; Dadashzadeh 2020; Sinha and Walton 2020 (Polygonal blocks)]. Christianson et al. (2006) used the method to conduct numerical triaxial testing of simulated lithophysal tuff samples to supplement existing uniaxial compressive strength tests (UCS) data; Gao (2013) used it to study the behavior of coal rock in comparison to the UDEC Trigon logic. Others (e.g., Ghazvinian et al. 2014; Zhu et al. 2017) used the method to investigate the mechanical behavior of hard rocks. In all of these studies, a calibration process was employed. Consequence to these observations, the BBM method is employed in this study to analyze these mechanisms and the pillar rib stability.

2 The Strength Reduction Method

The foundation of this work is built upon the SRM. The ease with which results from the strength reduction method can be interpreted has made the method the preferred choice for rock structure stability analysis. Current empirical safety factor calculations are done using the load to capacity comparison. But as observed by Esterhuizen (2012), deploying this classic method to study the stability of coal pillars may be problematic. This is because there is no clear definition of which load to use in the calculation due to load or stress redistribution. Additionally, the capacity of the structure is not easily defined when support is present. This deduction can be applied to the problem of coal rib stability analysis.

The strength reduction method has received great acceptance in the stability analysis of slopes and other engineering structures. The method has become even more reliable with the increasing power of computers. In the SRM process, a factor of safety is evaluated as a gradual reduction of the mechanical strength properties of the rock mass until instability in the model is reached. The limiting value at which failure occurs is taken as the FS. The SRM is a fairly new procedure and was first used by Zienkiewicz et al. (1975). Since then, more researchers have employed it in various studies, including (Naylor 1982; Giam and Donald 1988; Ugai and Leshchinsky 1995; Dawson et al. 1999; Griffith and Lane 1999; Lorig and Varona 2000; Cala and Flisiak 2003; Zheng et al. 2005; Cheng 2007; Zheng et al. 2009 and others). Esterhuizen (2012) applied the method in a continuum model to investigate the effectiveness of different support in coal mines. Tulu et al. (2016) adapted the method to study entry stability in

complex multiple-seam conditions. Esterhuizen's (2012) and Tulu's (2016) studies elicited the fact that continuum mechanics-based modeling of rock support structures does not capture the complete complex interaction between support and the rock material. It is because continuum-based numerical models lack the ability to capture the large-scale deformation and also the splitting, rotation of rock materials.

A factor of safety is often employed in the design of coal mine pillars. This factor is computed based on estimated strength and overburden load acting on the pillar. It can be demonstrated that the SRM has added advantages over the current empirical analysis of *estimated strength over assumed load*. Apart from a considerable reduction in the number of assumptions, in the SRM, the failure mechanism and the location of the failure surfaces can be visualized. This knowledge will inform ground control decision making to mitigate pillar failures. Additionally, the SRM can give information such as stresses and ground displacement/movements, which are not possible with the empirical methods. The key to fully harnessing the superior advantages of the SRM is the deployment of the right numerical tool, input parameters, and a clear definition of what constitutes failure. There are several criteria available to define what constitutes model instability in the SRM. These methods, however, only define structural failure when they develop copiously in the model. Examples of these methods are: (1) the connectivity of plastic zone in the case of continuum modeling; (2) tensile and shear fracture coalescence in the bonded block modeling (BBM) scenario (Sunkpal et al. 2020); and (3) the non-convergence of the numerical solution and rapid mutation of deformation.

Details of the working process of the SRM can be found in (Itasca 2019). Here is a brief summary of the procedure as applied in this study. In this process, the FS is calculated automatically by performing a series of simulations while changing the strength properties of the coal pillar to establish a limiting state where there is a numerical instability. The FS is taken to be the strength reduction factor (SRF) at which this failure or instability occurs. At this point, the failure mechanism is also established. Since the mechanical behavior of the BBM is controlled by the micro-properties of the contact areas between blocks, the SRM is applied to the strength parameters of the contacts. These contact micro-properties are the cohesion, c, friction angle, φ and/or tensile strength, σ_t. In applying the SRF for any geotechnical structure, a series of simulations are performed using trial SRFs by adjusting the values of the strength parameters: cohesion, friction, and/or tensile strength. This is done progressively to bring the structure to the point of instability where numerical convergence is no longer possible. According to the coulomb-slip model implemented for the BBM, scaling of the strength is possible by applying a strength reduction factor (SRF) to strength parameters: The following Eqs. 1–3 are implemented in the scaling process.

$$c_{new} = \frac{1}{SRF} \times c \tag{1}$$

$$\varphi_{new} = \arctan\left(\frac{1}{SRF} \times \tan(\varphi)\right) \tag{2}$$

$$\sigma_t = \frac{1}{SRF} \times \sigma_t \tag{3}$$

Though there is an inbuilt command for the factor of safety analysis in UDEC, it is not used in this study because it is mostly applied to elasto-plastic materials. Instead, the SRM procedure is implemented in UDEC using the internal FISH programming language. This study is using the BBM approach in which the strength of the rock mass is controlled by the contact properties between the blocks. Consequently, the strength of the coal pillar properties is reduced using the inbuilt FISH language in UDEC. This approach also gives the researchers the freedom to control the modeling process.

3 Numerical Modeling

Continuum and discontinuum modeling methods are usually used in solving most rock engineering problems. Though there have been some studies of rock spalling and buckling studies using continuum models (Hajiabdolmajid et al. 2002; Mohamed et al. 2016; Gale et al. 2004), this technique is inherently limited when the rock behavior involves degradation in the form of spalling and buckling, two most prominent failure mechanisms in coal ribs (Lorig and Varona 2013). An additional limitation of continuum modeling is demonstrated in tunnel breakout modeling undertaken by Martin (1997). Martin (1997) demonstrated the dilemma of using continuum modeling to predict failure. As noted by Barton and Shen (2017), continuum models failed to model the mechanisms of the so-called *main event*: extensional-strain fracturing followed by discontinuous propagation in shearing under high-stress levels. Laboratory test results in combination with a numerical calibration technique is used to determine inputs for the numerical models. As previously stated, the BBM approach is suitable for this study owing to its ability to simulate the initiation of cracks that coalesce and propagate, resulting in extension and shear fracturing. The BBM method is implemented in the Universal Distinct Element Code (UDEC) software to study the coal rib stability. This investigation is focused on only the rib of the coal pillar. The modeling is focused on: (1) examining the mechanisms of failure in the rib, (2) examining lateral deformation of the rib, and (3) exploring the coal mass support

interaction behavior. Safety factors are then computed for the rib in both the supported and unsupported scenarios.

3.1 Mechanical Properties Calibration for in-situ Modeling

In this study, the coal rib is discretized into small blocks using the Voronoi tessellation logic. The coal seam and immediate roof and floor sandstone are represented as an assembly of polygonal, elastic blocks bonded together across their boundaries to form a coherent non-cleated rib. In this setup, blocks are bonded at their contacts with cohesion and tensile strength. Figure 1a illustrates the Voronoi tessellation division, the properties that govern the failure of the contacts, and the emergent macroscopic behavior of the model (Fig. 1b). The Coulomb friction law governs the mechanical behavior of the contacts bounding the blocks. In this method, cracks initiate and grow along the boundaries of blocks when the maximum stress exceeds tensile or shear strength thresholds. This concept is expressed by the following Eqs. 4–6:

$$\Delta\sigma_n = -k_n \Delta u_n \tag{4}$$

$$\Delta\sigma_s = -k_s \Delta u_s \tag{5}$$

$$|\tau_s| \leq C + \sigma_n \tan(\varphi) \tag{6}$$

$\Delta\sigma_n$ is the change in normal stress, k_n is the normal stiffness, Δu_n is the incremental normal displacement, $\Delta\sigma_s$ is the change in shear stress, k_s is the shear stiffness, Δu_s is the incremental shear displacement, and C and φ are the cohesion and joint friction angle, respectively. A broader explanation of this contact behavior can be found in Lorig and Cundall (1989) and Itasca (2019).

The material behavior of the BBM is controlled by micro-mechanical properties (Fig. 1a). Because these micro-properties cannot easily be measured in the laboratory, they are often determined by employing a calibration process in which Uniaxial and Brazilian Compression tests are run to match with results of previously conducted laboratory tests. The procedure involves an iterative variation of the micro-mechanical properties of the Voronoi model to match existing laboratory measured stress–strain results. This study employed the calibration process described in Christianson et al. (2006), Gao (2013), Zhu et al. (2017).

The in-situ rock and coal mass macro-properties were derived using empirical formulas (Zhang and Einstein 2004). The properties of the coal seam were taken from the laboratory test conducted by Rusnak (2017) on the Central Appalachian high volatile coal beds. Rusnak attested to the suitability of these results for rock mass classification system to address coal pillar rib stability challenges. An RQD of 70% was used for the coal and 80% for the roof and floor sandstone rock from which the in-situ deformation modulus was determined using Eq. (7) (Zhang and Einstein 2004). These RQD values agree with data ranges for coal and sandstone in published literature. Singh and Seshagiri (2005) determined the ratios of uniaxial compression strength and deformation modulus of intact rock to in-situ rock modulus to have a strong linear correlation in numerous uniaxial compression tests. They formulated the relationship presented in Eq. (8). The strength of the in-situ rock and coal mass is calculated using Eq. (8):

$$\frac{E_m}{E_i} = 10^{0.0186RQD - 1.91} \tag{7}$$

$$\sigma_m = \sigma_i \times \left(\frac{E_m}{E_i}\right)^n \tag{8}$$

E_m and E_i are rock mass and intact rock deformation moduli, respectively; n is a data fitting parameter representing inverse gradient, which is 0.56 for splitting and shearing, 0.66 for sliding, 0.72 for rotation, 0.63 for an average of all modes of failure; and σ_m and σ_i are rock mass and intact rock uniaxial strength, respectively. The UCS model failure was dominated by splitting and shearing in this study, thus a constant of 0.56 was used in downgrading the laboratory UCS and Youngs modulus properties to the in-situ properties. The tensile strength of the rock mass was taken as ten percent of the uniaxial compressive strength.

As indicated previously, the behavior of the model is controlled by the micro-properties (Fig. 1a). These micro-properties are grouped into two and referred to as the strength parameters comprising friction angle, tensile strength, and cohesion; and elastic parameters which are the bulk and shear modulus of the blocks as well as normal and shear stiffness of the polygonal contacts. Uniaxial Compression Tests (UCTs) and Brazilian Tensile Tests (BTTs) samples of dimensions 0.6 m × 1.5 m rectangle and 0.6 m diameter disk were built to model the in-situ coal mass strengths and tensile strength, respectively (Fig. 1a). The target properties for these tests are listed in Table 1. An average Voronoi edge length of 0.08 cm and 0.15 cm were used for coal and sandstone, respectively. Prior studies recommended that these edge lengths should be small enough to allow at least 10 blocks across the width of the model to permit realistic fracturing in the model (Kazerani and Zhao 2010; Gao 2013; Lisjak and Grasselli 2014; Fabjan et al. 2015; Zhang et al. 2018). Additionally, because the large in-situ model also takes the same grain size, it should be chosen to ensure the numerical efficiency of these models. The tests are conducted by applying a constant velocity of 0.01 m/s at the bottom and top of the two frictionless, elastic platens

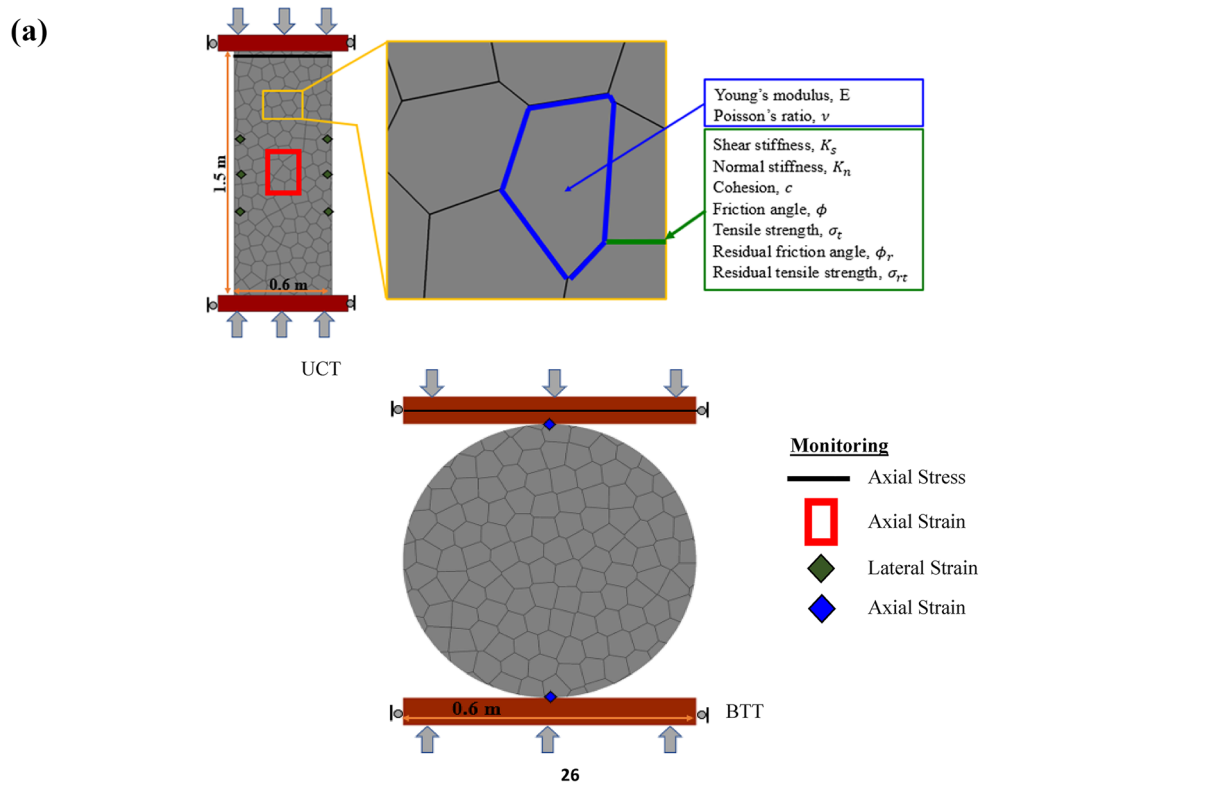
(a)
1.5 m
0.6 m
Young's modulus, E
Poisson's ratio, ν
Shear stiffness, K_s
Normal stiffness, K_n
Cohesion, c
Friction angle, ϕ
Tensile strength, σ_t
Residual friction angle, ϕ_r
Residual tensile strength, σ_{rt}
UCT
Monitoring
Axial Stress
Axial Strain
Lateral Strain
Axial Strain
0.6 m
BTT
26

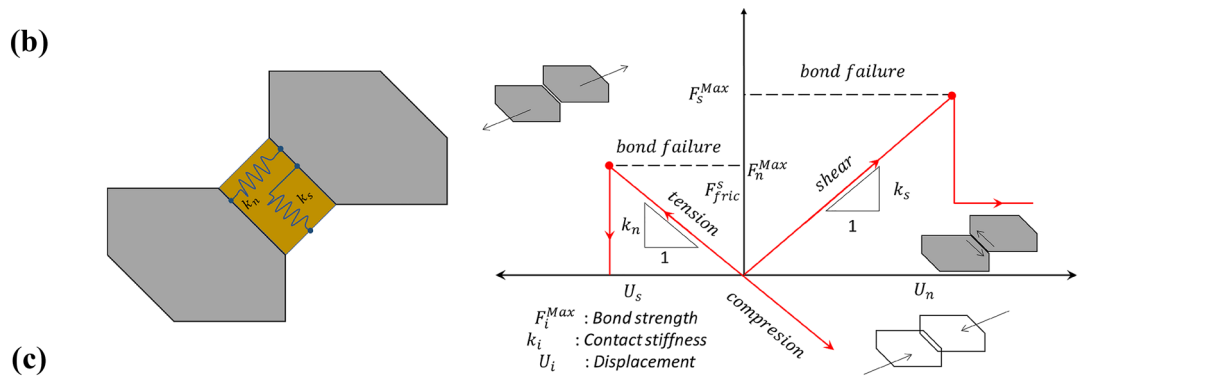
(b)
bond failure
bond failure
shear
tension
compresion
F_s^{Max}
F_n^{Max}
F_{fric}^s
k_n
k_s
1
1
U_s
U_n
F_i^{Max} : Bond strength
k_i : Contact stiffness
U_i : Displacement

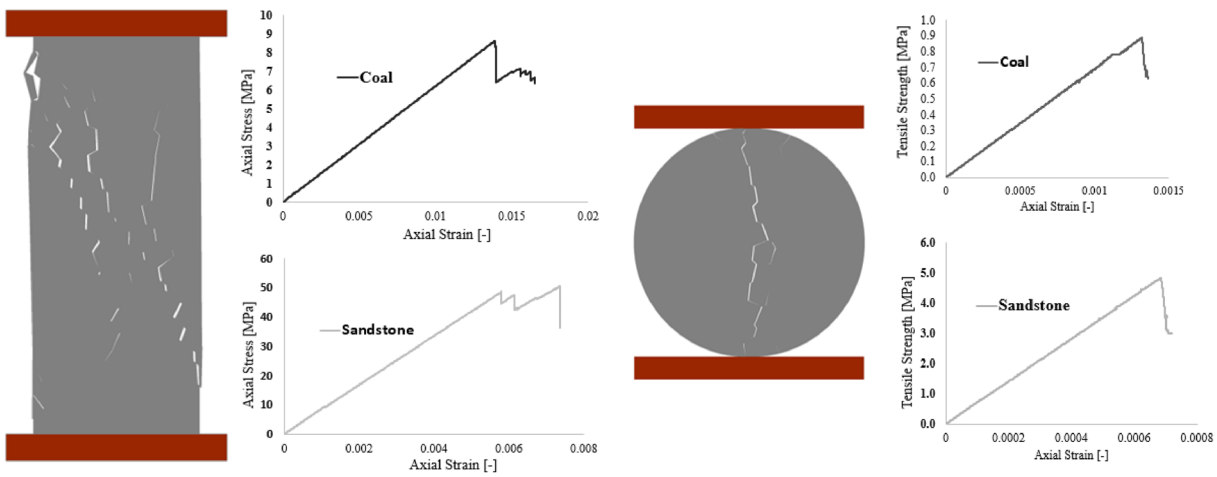
(c)
Coal
Axial Stress [MPa]
Axial Strain [-]
Sandstone
Axial Stress [MPa]
Axial Strain [-]
Coal
Tensile Strength [MPa]
Axial Strain [-]
Sandstone
Tensile Strength [MPa]
Axial Strain [-]

◂**Fig. 1** Configuration of the UDEC Voronoi model used for simulating in-situ strength and results of the laboratory experiments (**a**) shows the models with the micro properties locations in the sample that controls Voronoi models behavior (**b**) illustrations of the constitutive behavior of the Voronoi blocks, normal and shear stiffnesses between contacts *(left),* shear and tension failure criteria of its contacts *(right)* (b is redrawn after Lisjak and Grasselli 2014) (**c**) simulated uniaxial compression test (*UCT*) and Brazilian tensile test (*BTT*) showing the calibrated compressive -and tensile stress–strain responses and observed sample damage evolution

(Fig. 1a). A servo control function is applied to maintain the mean stress constant during the numerical experiments. The loading rate is small enough to ensure quasi-static equilibrium is maintained during the test (Farahmand and Diederichs 2015). Table 2 presents a comparison of the Young's modulus, peak axial stress, and peak tensile stress obtained from the experiment and simulation. The maximum error for the Young's modulus, UCS, and BTS is 5.52%, 0.82%, and 2.24%, respectively, which are relatively small. The calibration accuracy between the experimental stress–strain curve and the simulated stress–strain curve is reasonable. The calibration process conducted in this study for the in-situ rock and coal mass yielded the properties presented in Table 3, and the stress–strain curves obtained tests are shown in Fig. 1c. The bulk and shear modulus of the blocks were calculated using Eqs. 9, 10, while the normal and shear stiffness of the contacts were determined using Eq. 11 (Itasca 2019). The shear and normal stiffness are related by the ratio presented in Table 3 as determined from the calibration process.

$$K = \frac{E_m}{2(1-\nu)} \tag{9}$$

$$G = \frac{E_m}{2(1+\nu)} \tag{10}$$

$$k_n = b\frac{K + \frac{4}{3}G}{\Delta Z_{\min}} \tag{11}$$

K and G are the bulk and shear modulus, respectively, E_m is the Young's modulus, ν is Poisson's ratio, $\Delta Z_{\min}$ represents the smallest width of the zone adjoining the contact in the normal direction, and b is a factor that ranges between 1 and 10.

Martin and Chandler (1994) showed that cohesion and friction are not mobilized simultaneously in brittle failure of rock. Through laboratory triaxial tests, they demonstrated that as damage accumulates, the cohesive component of shearing degrades while the frictional component mobilizes. Hajiabdolmajid et al. (2002) successfully implemented the cohesional weakening-frictional strengthening (CWFS) behavior in a continuum modeling to simulate notch formation around the tunnels of deep underground openings in massive brittle rocks. This was after they observed that the conventional material models failed to reproduce the mechanisms of progressive failure observed around the tunnels. The rib failure behavior is a gradual and progressive damage process, just as observed by Hajiabdolmajid et al. (2002) in the tunnels. Other works, including Diederichs (2007b), Edelbro (2009), and Walton and Diederichs (2015) presented studies to support the application of the CWFS model for modeling progressive brittle failure of rocks. The CWFS concept for the contact behavior between the grains in the BBM is adopted by defining the cohesion, c and residual friction angle, ϕ_r for the contacts while setting the residual cohesion, c_r, and friction angle, ϕ to zero as presented in Table 3 (Ghazvinian et al. 2014).

3.2 Model Generation and Boundary Conditions

A numerical model with dimensions of 40 × 40 m was built to investigate how the coal rib responds to mechanical loading (Fig. 2). The vertical boundaries of the model were fixed in the x-directions and the bottom horizontal axis was fixed in the y-direction to prevent movements and rotations along these directions. A stress boundary condition was applied at the top of the model to achieve the desired simulated depth. To reduce computational time, the Voronoi tessellation logic was used around the coal rib area only, 7 m from the ribline. The vertical interface connecting the coal to the elastic region of the pillar was given the calibrated coal micro-properties. The average edge length of 0.08 m was assigned to the polygonal Voronoi blocks in the pillar. The surrounding rock mass in the immediate roof and floor of the rib was discretized using relatively courser blocks with an average edge length of 0.15 m. The interfaces connecting the coal to the roof and floor materials were assumed to have a friction angle of 30° and cohesion of 0.57 MPa (Mohamed et al. 2019). The rest of the model is assumed to behave elastically. It has long been established that in-situ stress is a significant factor that affects the design, construction, and stability of underground excavation structures (Saati and Mortazavi 2011, Nasehi and Mortazavi 2013). The stress tensor components are always different at different orientations, and this variation plays an important role in the stability of rock excavations (Hijazo and González De Vallejo 2012; Yaméogo et al. 2013). The rib was assumed to be buried 250 m deep and thus, the vertical stress imposed on the upper boundary was calculated as 6.25 MPa with a stress gradient of 0.025 MPa/m. The in-situ stresses in the coal seam were initialized using the equations proposed by Liu et al. 2016 (Eqs. 12 and 13), while the in-situ stresses in the rock layers used the recommendations of Esterhuizen (2017) (unpublished) in Mohamed et al. (2019) (Eqs. 14 and 15).

Table 1 Simulation parameters for coal and rock specimens

Material properties	Intact rock/coal properties		Rock and coal mass properties	
	Coal (from Rusnak 2017)	Sandstone (from Nie 2011)	Coal	Sandstone
Density (kg/m^3)	1264.52	2200	1264.52	2200
Young's modulus (GPa)	2.55	23.44	0.63	8.87
Uniaxial compressive strength (MPa)	19.70	84.30	8.99	48.90
Tensile Strength (MPa)	1.31	8.43 (10% of UCS)	0.9 (10% of UCS)	4.90 (10% of UCS)
RQD (%)	–	–	70	80

Table 2 Comparison between experimental and simulated Young's modulus, UCS, and BTS values

Lithology	Young's modulus (GPa)			UCS (MPa)			BTS (MPa)		
	Experiment	Simulation	Error (%)	Experiment	Simulation	Error (%)	Experiment	Simulation	Error (%)
Sandstone	8.87	8.38	−5.52	48.9	48.5	−0.82	4.90	4.79	−2.24
Coal	0.63	0.62	−1.59	8.99	8.60	−4.34	0.90	0.88	−2.22

Table 3 Calculated micro-mechanical properties for the laboratory and in-situ strength of the coal and sandstone rocks

	Properties	Coal mass	Rock mass
Rock matrix	Young's modulus (GPa)	2.0	18.0
	Poisson ratio (−)	0.25	0.30
Contact	Shear stiffness, K_s (GPa/m/m)	150.0	250.0
	Normal stiffness, K_n (GPa/m/m)	405.0	2760.0
	K_s/K_n	0.37	0.10
	Cohesion, c (MPa)	9.0	26.0
	Friction angle, ϕ (degrees)	0.0	0.0
	Tensile strength, σ_t (MPa)	2.10	12.0
	Residual friction angle, ϕ_r (degree)	30.0	35.0
	Residual tensile strength, σ_{tr} (MPa)	0.0	0.0
	Residual cohesion, c_r (MPa)	0.0	0.0

$$\sigma_{cmax} = 1.174 + 0.024 \times Z_c \tag{12}$$

$$\sigma_{cmin} = 0.018 \times Z_c - 1.475 \tag{13}$$

$$\sigma_{rmax} = 0.313 + 0.027 \times Z_r + 0.000278 \times E_r \tag{14}$$

$$\sigma_{rmin} = 0.75 \times \sigma_{rmax} \tag{15}$$

σ_{cmax} and σ_{cmin} are the maximum and minimum horizontal stresses in MPa, respectively, and Z_c is the depth of coal seam in meters. σ_{rmax} and σ_{rmin} are the maximum and minimum horizontal stresses in MPa, respectively, E_r is the Young's modulus of rock strata in GPa, and Z_r is the depth of rock strata in meters.The model was initially brought to equilibrium under these in-situ stress conditions before the roadway was excavated. Before the supports were installed, the model was solved elastically to satisfy a second equilibrium state. This was done to account for the initial elastic deformation that occurs before the supports can be installed.

Determining a stable and unstable rib in this study was undertaken by observing a number of parameters, including the amount of the rib velocity, lateral and axial displacements, and the amount of contact or joint failure development and propagation. But as noted earlier, none of these criteria can be used solely for reliably evaluating the stability of the models. Therefore, in this study the transition from a stable to unstable rib has been assessed through a combination of these parameters. Figure 3 demonstrates an example of a velocity history plot used along with other established criteria to evaluate model stability. Figure 12 also presents a clear example of how the model stability is determined.

There is a definite presence of fractures in coal seams. However, coal strength is often estimated as an arbitrary fraction of the strength properties of the coal material. This is not surprising as it is still a challenge to realistically estimate the strength of rock mass, coal not an exception. One important coal mass property that is often ignored in assessing its strength is the inherent jointing system. Cleats and beddings are typically present in coal seams and have been confirmed to significantly impact the stability of coal pillars and ribs (Smith 1992; Kalamaras and Bieniawski 1993; Shepherd 2002; Kim and

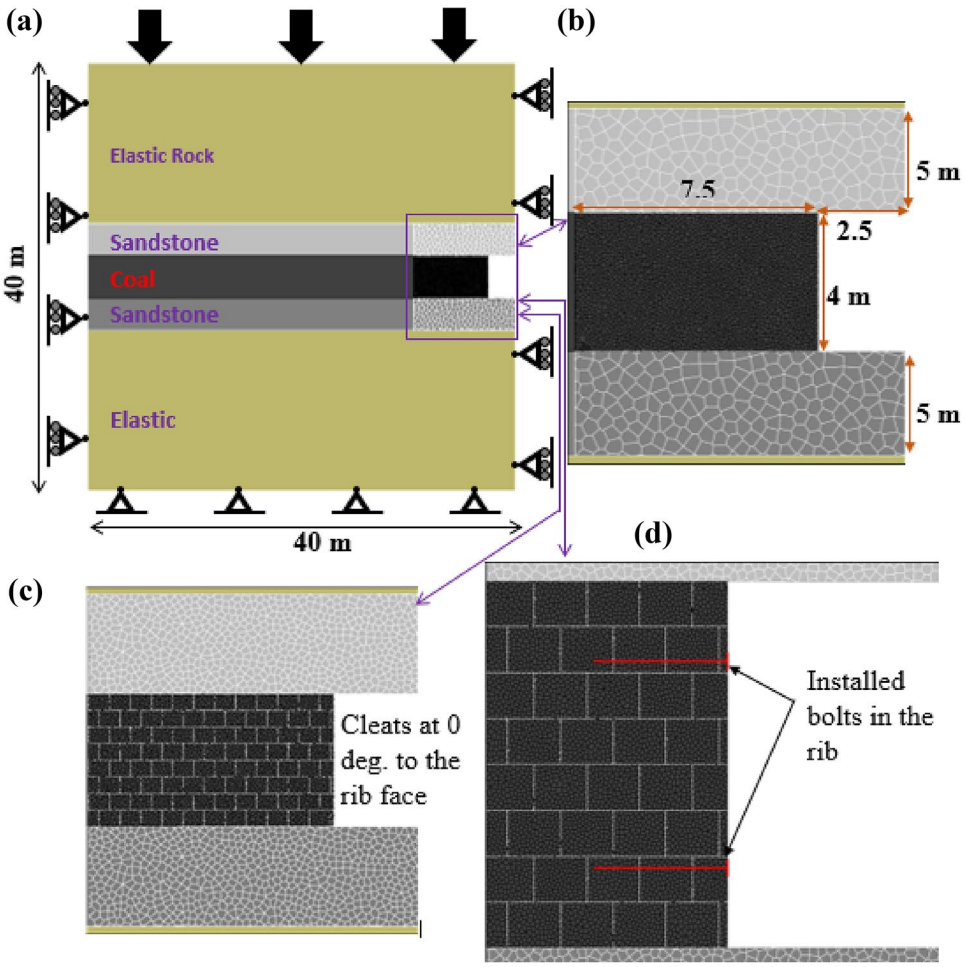

Fig. 2 Model geometry configuration used for the investigation of coal rib behavior (**a**) Non-cleated coal rib with no joint system. **b** Rib with joint/cleat system. **c** Jointed rib with installed bolts

Larson 2017; Heritage 2019; Vardar et al. 2019). It is in this respect that this research is taking a fundamental step in investigating their effect on coal rib stability. Face and butt cleats are mutually orthogonal and also perpendicular to the bedding planes (Laubach et al. 1998). The bedding spacing can range between millimeters to decimeters (Laubach et al. 1998). However, it is impractical to represent this level of precision of bedding plane spacing in this study. Therefore, bedding spacing was assumed to be 0.5 m, which agrees with field observations in Australian coal mines (Vardar et al. 2019). Vertically dipping cleats were also incorporated into the models at a constant spacing of 0.6 m. The bedding planes and vertical cleat were assumed to have zero cohesion and tensile strength with a friction angle of 20° (Esterhuizen, 1998; Sainsbury, 2008). The same normal and shear stiffness values were used for the joints and coal contacts to prevent block overlapping and fictitious stress concentrations. The orthogonal cleated coal seam is the most prevalent in the mines hence the decision to pilot this study with it (Fig. 2).

4 Numerical Modeling Results

A set of four DEM numerical models: (a) a non-cleated coal rib and (b) a coal rib with explicitly defined orthogonal cleats/joints in the coal seam, were modeled and analyzed (Fig. 2). These were analyzed as supported and unsupported cases to highlight the effect of support and cleats on rib performance. The failure mechanism of the rib was evaluated by analyzing the rib failure mechanisms, examining lateral deformation in the rib, and exploring the coal mass and support interaction behavior with respect to the rib stability.

4.1 Stability Analysis of the Unsupported Non-cleated Coal Rib

The simulated damage process of the non-cleated coal rib is presented in Fig. 4. After the excavation (Fig. 4a), shear and tensile fractures initiate around the coal rib near the roof and floor corners. The tensile cracking also initiates at this stage. It is important to observe that the maximum depth of fracturing in the rib is fully developed at a strength reduction factor (SRF) of 1.4 (Fig. 4e). This depth is about

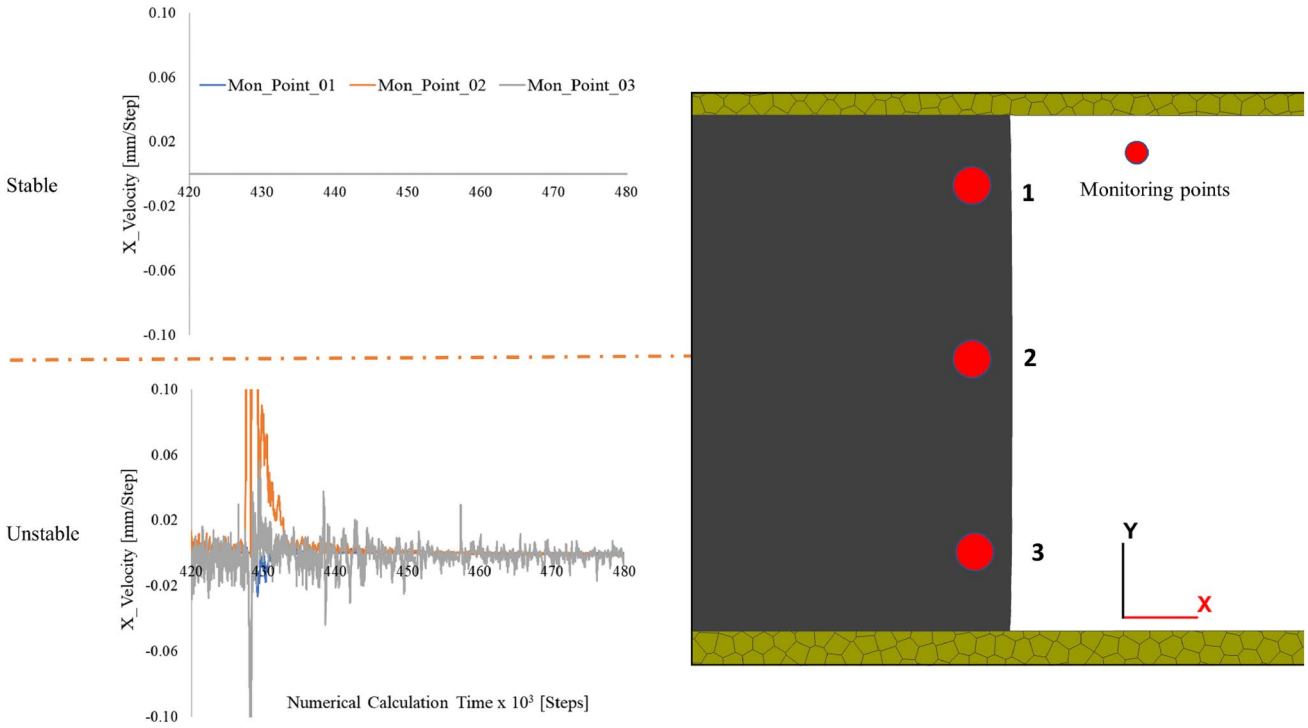

Fig. 3 Model stability determination using velocity history plots

1.4 m measured from the rib side into the rib. Further reduction beyond this SRF resulted in the formation of a large fractured zone in the coal rib where the coal is extensively fractured, and the rib became unstable. There are occasions where mine operators are unsure what length of bolt/cable to deploy to improve rib performance. These observations present a great opportunity to answer such critical questions for the industry. Additionally, worth noting is the development of short tensile fractures and their coalescence with a further reduction of the coal mass strength to form fractures that are subparallel to the rib line. As can be seen in Fig. 4, the fracture front tends to propagate in shear and coalesce with each other to form larger fractures. The fracture initiation and propagation developed progressively deeper into the ribs. The modeling results demonstrated the potential of the UDEC Voronoi logic to capture the crack development, propagation, and coalescence of these cracks in the coal rib. Typical rib failure mechanisms, such as spalling, shear failure, guttering, and buckling can be realistically reproduced by using the UDEC Voronoi logic.

The fracture development (Fig. 4) and mobilized zone deformation (Fig. 5 top row) explain the rib damage boundaries matches with the lowest stress concentration areas in the rib (Fig. 5 bottom row). The analysis presented in this section highlights the critical possibility of utilizing this block-based model to predict coal rib fracturing, coal rib deformation, and the all-important depth of fractured or mobilized zone. The knowledge could be very significant in guiding ground control engineers and mine operators to plan and optimize the rib support requirements to improve the safety of miners.

4.2 Stability Analysis of the Unsupported Cleated Coal Rib

Figure 6 presents the results of the cleated coal rib. It is observed that the crack propagation in this rib has more shear failure when compared with the non-cleated coal rib, but ultimately the rib failure is dominated by tensile fracturing. The increase of observed shearing in cleated rib might explain the reduced depth of fracturing. The presence of joints or cleats can result in the release of some strain energy through joint deformation and sliding. This absence of stored energy buildup can reduce the potential violent failure. Also, it is worth noting that the depth of fracture at SRF of 1.40 before failure is 1.15 m. This is lower than the depth of fracture before failure of 1.4 m calculated for the non-cleated rib case at a strength reduction of 1.48. It can be explained that the presence of cleats definitely inhibits the depth of fracture development. Also, as expected, the marginal factor of safety (FS) of the non-cleated rib of 1.41 is higher than the cleated rib of 1.30. The presence of cleats weakens the coal mass strength.

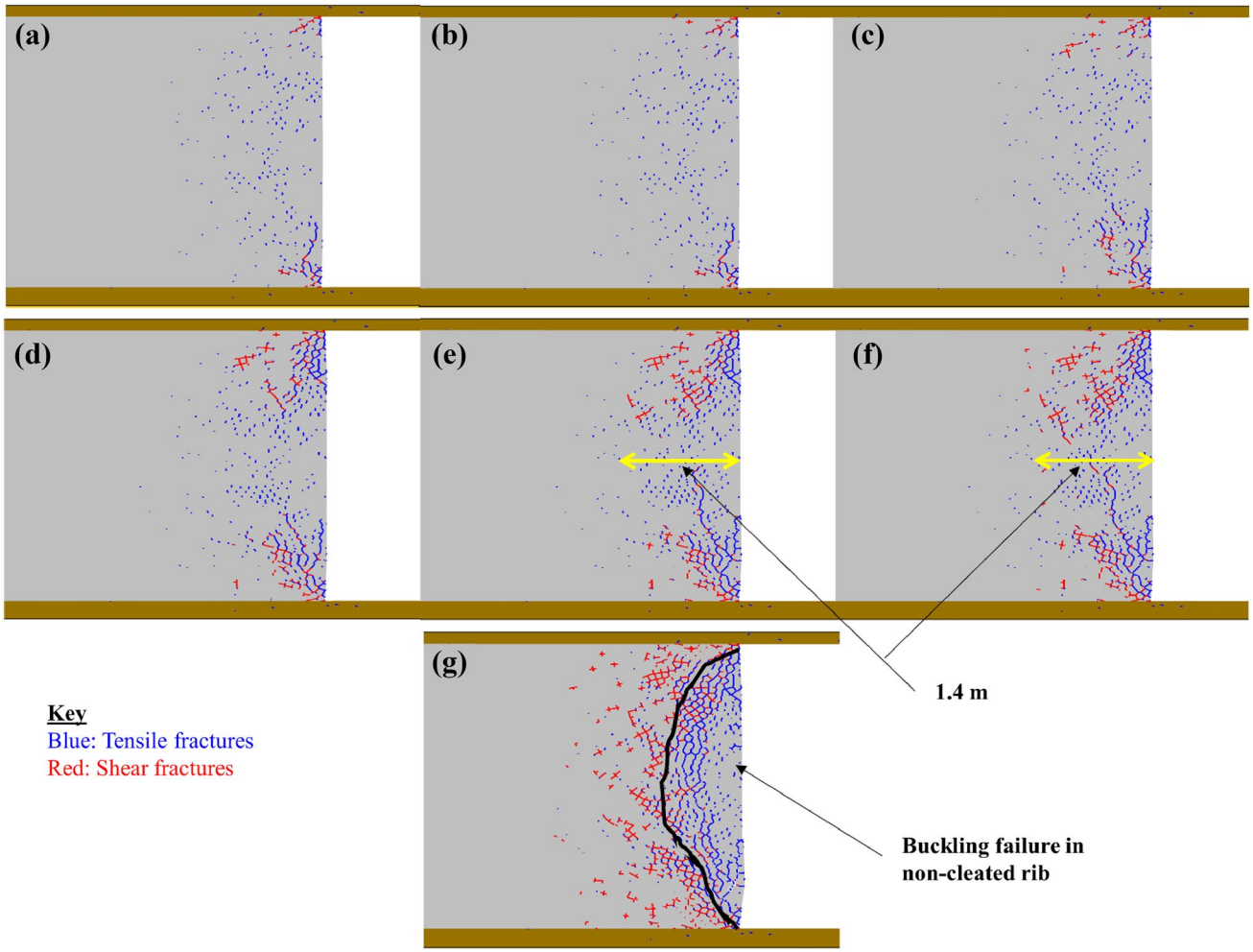

Fig. 4 Non-cleated rib failure evolution as the coal mass strength properties are gradually reduced, tensile cracks are in blue and shear in red. **a** is the base case and the rib status after excavation and solving to equilibrium, (**b**), (**c**), (**d**), (**e**), (**f**), and (**g**) are the cases at strength properties reduction of 1.10, 1.20, 1.30, 1.40, 1.48, and 1.50 (unstable case)

One significant observation worth noting in the preceding sections is the fact that there is no discernible failure of the roof and floor rock mass in the results presented. In practical terms, based on the authors' communication with experienced ground control engineers, rib stability challenges are often found in the competent roof and floor geologic settings. Nevertheless, in the analysis of rib stability, just like in pillar studies, the problem should be treated as a system where the rib, roof, and floor rock mass are considered together. In the event that the roof and floor rock mass does not yield considerably, as is the case in this study, the strength and therefore the stability of the coal rib, to a good measure, is still dependent on their mechanical performance.

4.3 Stability Analysis of the Supported Non-cleated and Cleated Coal Rib

The interaction of support and the coal mass is evaluated in this section. The intention is to present a foundation upon which future rib optimization studies will be conducted. This study will demonstrate how the bonded block model establishes, in explicit terms, this interaction. The support was modeled as a fully grouted rock bolt discretized into equally spaced segments in order to enable axial force and strain measurement on each of these reinforcing elements. Bolts were designed as 1.5 m long, 19 mm diameter bars at 0.875 m spacing from the host rock and spaced at 2.25 m in the pillar rib of 4 m

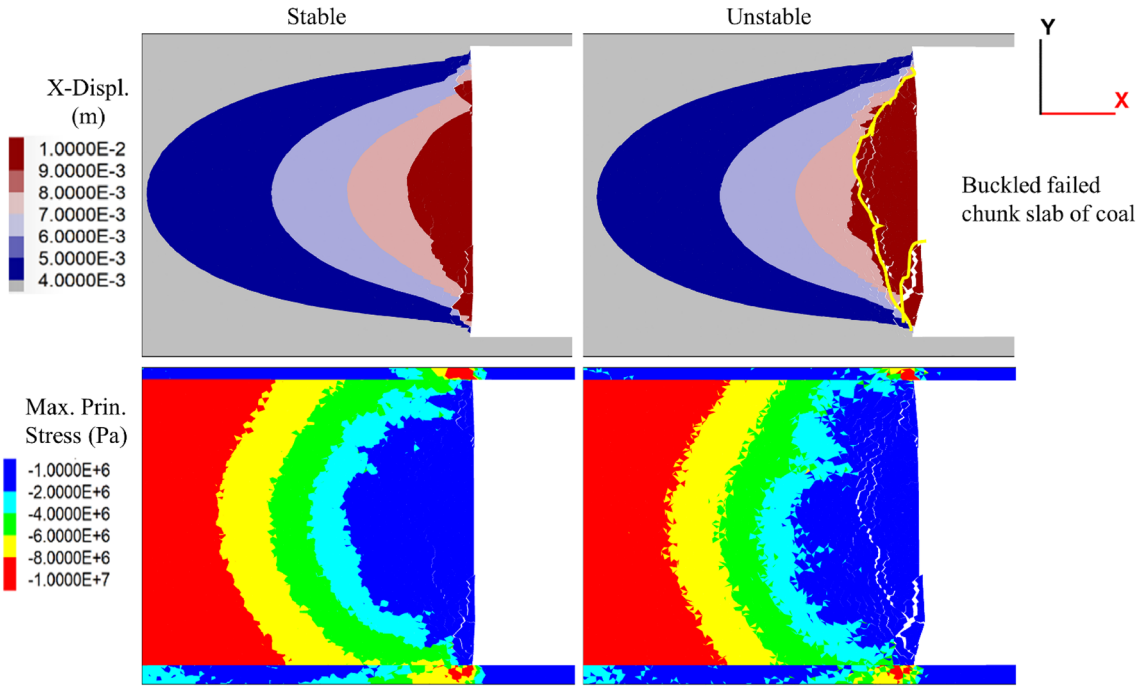

Fig. 5 Stability characteristics of the non-cleated coal rib at the stable SRF of 1.40 and the unstable SRF of 1.50. The top row depicts the lateral displacement, and the bottom row is the maximum principal stresses contour plots

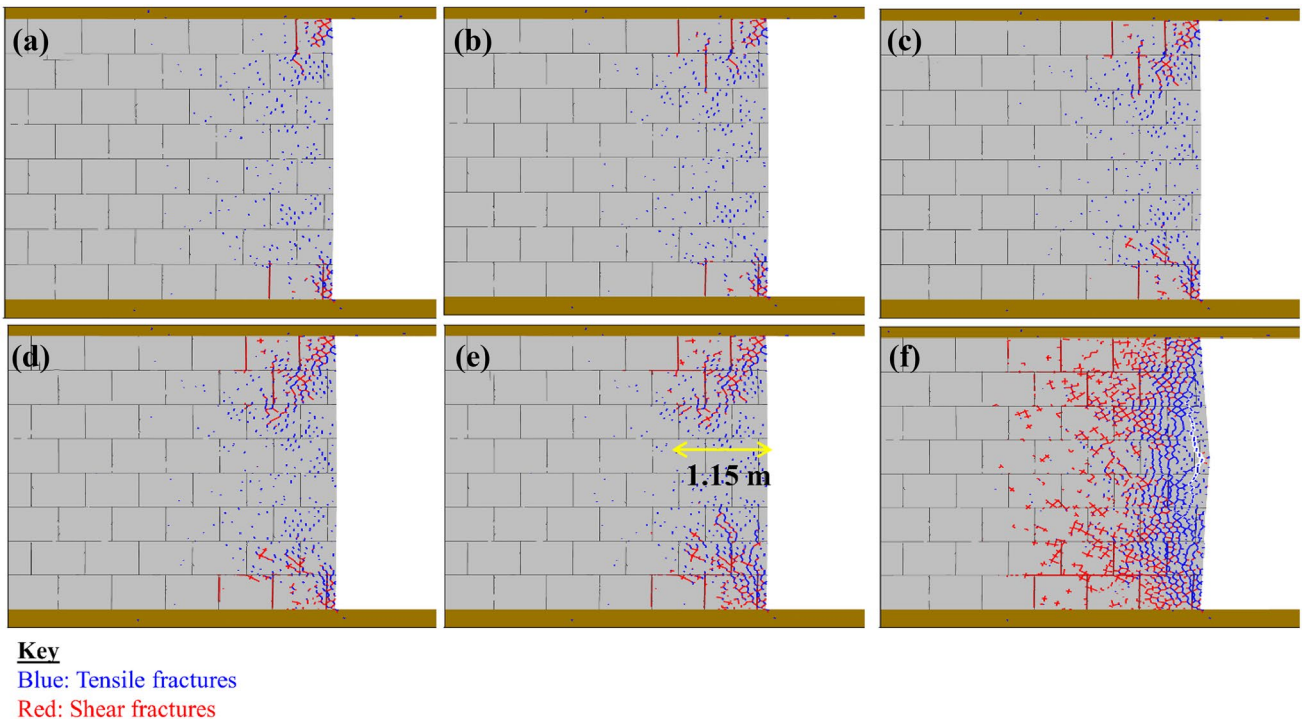

Fig. 6 Rib with cleats failure evolution as the coal mass strength properties are gradually reduced, tensile cracks are in blue and shear in red. **a** is the base case and the rib status after excavation and solving to equilibrium, (**b**), (**c**), (**d**), and (**e**) are the cases at strength properties reduction of 1.10, 1.20, 1.30, 14.0, and 1.41 (unstable case)

height. The maximum number of bolts per vertical rib bolt row often used in coal mines in the US is 2, according to a rib survey conducted by Mohamed et al. (2021). The spacing between the bolts was determined based on the initial failure patterns observed in the unsupported cases, while that between the roof and support was selected to enable enough space for the bolter. A steel plate of 0.2 m length was also simulated. The parameters used for the cable support are typical for coal mines in the US and were obtained from Zipf (2006). These are summarized in Table 4. Since this study did not have field data to compare with results from the models, the effect of the confinement provided by the support is evaluated based on the fracture development in the rib of the pillar as the strength of the coal mass is reduced. Additionally, the lateral rib deformation was analyzed to evaluate the performance of the rock bolts in the coal mass. The effect of the support on the fracture development in the rib is observed in Fig. 7. The non-cleated, unsupported rib ultimately failed at a strength reduction factor of 1.50 while the rib remained stable at higher strength reduction factors when support is introduced. A gradual increase in loading of the bolts in the strength reduction range of 1.70 to 1.80 was also observed since the support needed to bear more of the load to keep the rib stable as the coal mass weakens. As shown in Fig. 8, the fractured zone of the rib decreased dramatically when reinforcement was introduced. As seen in the deformation plots in Fig. 8c and d, the rib dilation is halted on the introduction of support. Also, note that the SRF used in Fig. 8 is the same SRF at which the non-cleated rib without support failed. In effect, introducing the support increased the serviceability of the rib under the same coal mass properties. Because the supports tend to limit the rib from relaxation, thus increased confinement, it is realized that the tensile fracture propagation is limited while there is an increase in shear crack generation. This highlights the confining effect provided by the installation of the support. The support suppressed the development of cracking and further lateral deformation (Figs. 7, 8, 9, and 10). The depth of softening before failure in these cases is lower, especially in the rib case with cleats (Fig. 10). The deformation in the non-cleated rib case is gradual until failure, indicating an impressive self-supporting capacity of the non-cleated rib. Figure 9 presents the damage process of the cleated rib. The FSs calculated for the supported cases are lower than the unsupported cases for the non-cleated rib. The presence of cleats makes the rock mass weaker unlike the non-cleated rib case, which is treated as an intact rock, a rarity in practice.

Table 4 Properties of support elements used in the BBM model

Cable					Grout			Beam				
Density [kg/m^3]	Young's modulus [GPa]	Yield stress [GPa]	Yield strength [kN]	Failure strain [%]	Stiffness K_{bond} [MN/m/m]	Shear S_{bond} [kN/m]	Shear modulus [GPa]	Young's modulus [GPa]	Yield stress [GPa]	Interface Normal Stiffness [GPa/m]	Interface Shear Stiffness [GPa/m]	Interface Friction [deg.]
7800.00	200.00	500.00	157.08	10.00	1.92	350.00	8.00	200.00	500.00	10.00	10.00	45

4.4 Evaluation of Rib Performance Using the Depth of Softening (DOS)

The rib behavior in terms of depth of softening (DOS) was also assessed. The DOS is the practical extent of lateral movement or softening within the coal rib (Cowell 2006). This is different from the absolute total rib displacement,

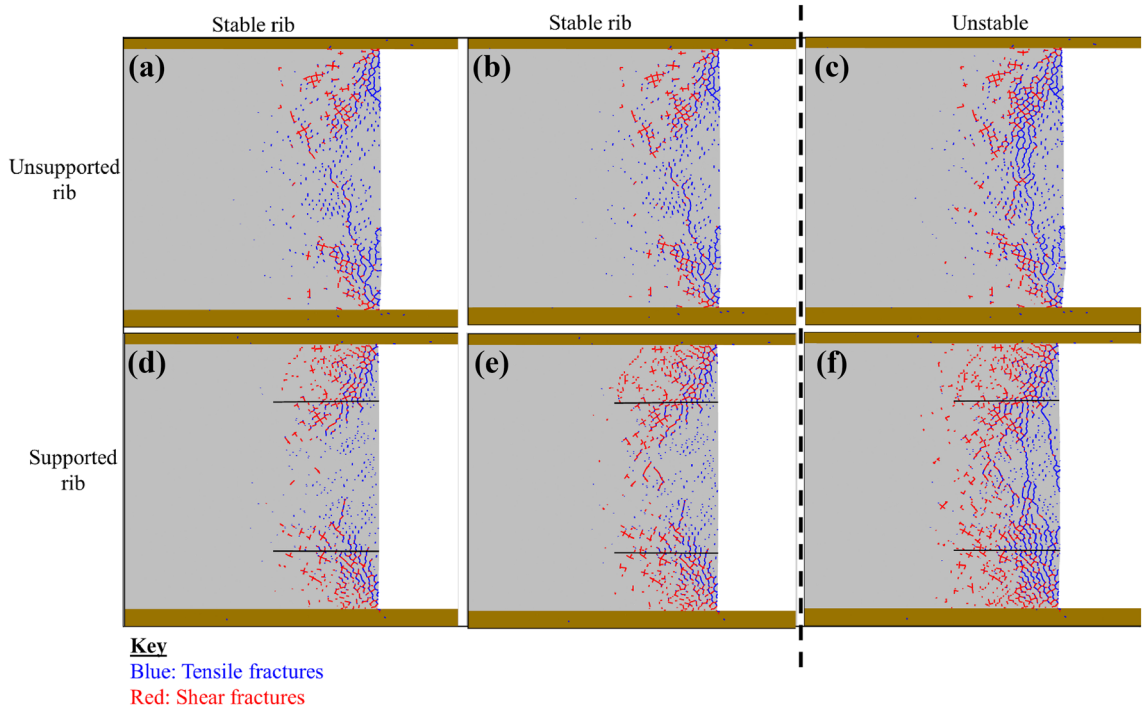

Fig. 7 Progressive damage process of the non-cleated coal rib as the strength properties are reduced. The top row a, b, c depicts the non-cleated rib without any support. The SRF calculated for a, b, and c are 1.47, 1.48, and 1.50, respectively. The bottom row presents the supported rib results. Calculated SRF for d, e, and f are 1.50, 1.60, and 1.70, respectively. The two models in the far right are the unstable cases for the supported and unsupported rib, i.e., c and f. Two models prior to failure and the failed rib were chosen to explain the stabilizing effect of rib support

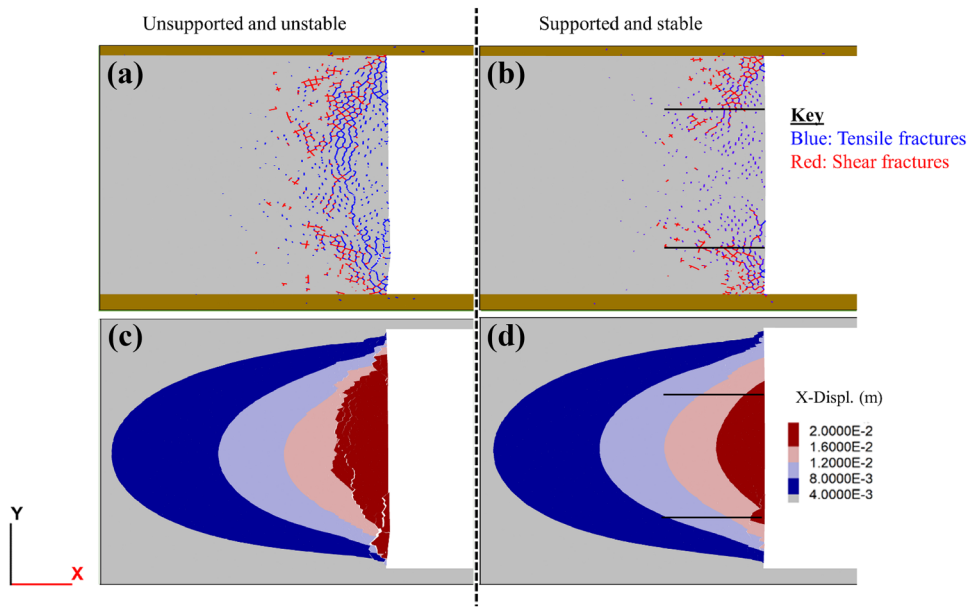

Fig. 8 Damage process of the non-cleated coal rib at applied strength reduction of 1.50 (**a**) and (**b**) are showing the fracture damage process, and (**c**) and (**d**) are showing the deformation damage process

which is simply the horizontal displacement of the ribline surface. Colwell's (2006) study cautioned against using the absolute total rib displacement in determining the DOS as it will lead to its over-estimation. Using extensometer data collected by Colwell (2006), the mobilized zone was recorded when absolute rib lateral displacement was approximately ~ 10 mm. In this study, 10 mm total rib displacement was used to estimate the DOS as depicted in Fig. 11. These results are for the stable cases for all four rib types investigated in this study. The DOS for the supported non-cleated

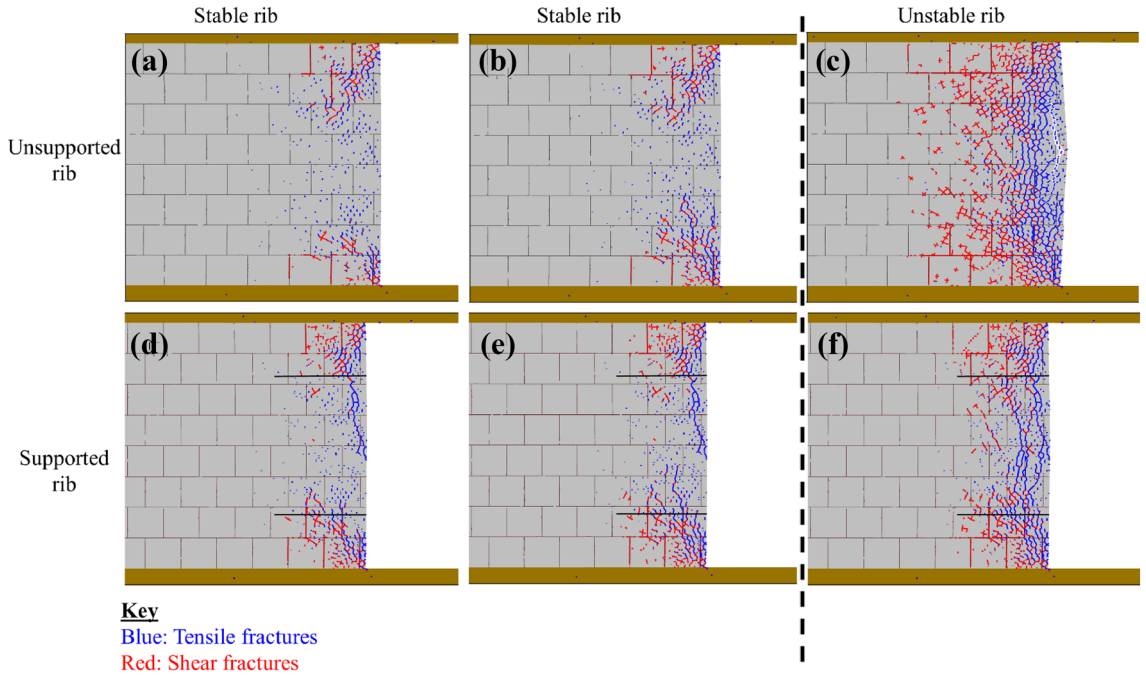

Fig. 9 Progressive damage process of the rib with a set of orthogonal joints as the strength properties are reduced. The top row a, b, c depicts the cleated rib without any support. The SRF calculated for a, b, and c are 1.30, 1.40, and 1.41, respectively. The bottom row presents the supported cleated rib. Calculated SRF for d, e, and f are 1.30, 1.40, and 1.50, respectively. The two models in the far right are the unstable cases for the supported and unsupported rib, i.e., c and f. Two models prior to failure and the failed rib were chosen to explain the stabilizing effect of rib support

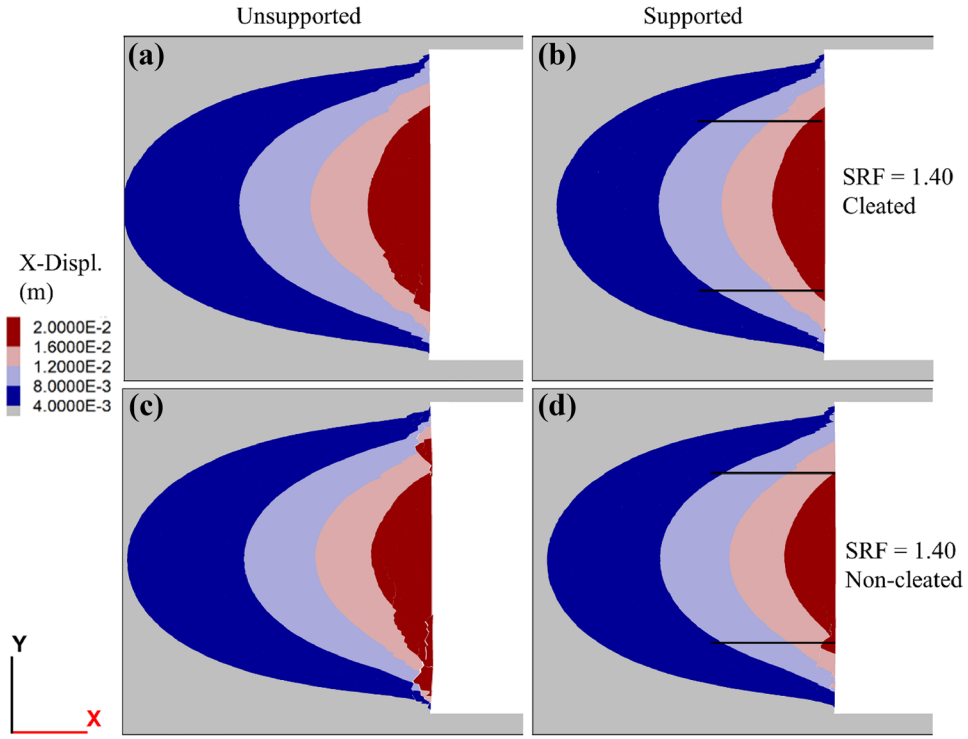

Fig. 10 Deformation stability characteristics of the coal rib (**a**) and (**b**) are cleated at a strength reduction factor of 1.40 and supported, and (**c**) and (**d**) are non-cleated rib at a strength reduction factor of 1.40. The chart to the right illustrates the depth of softening (DOS) estimation for these ribs

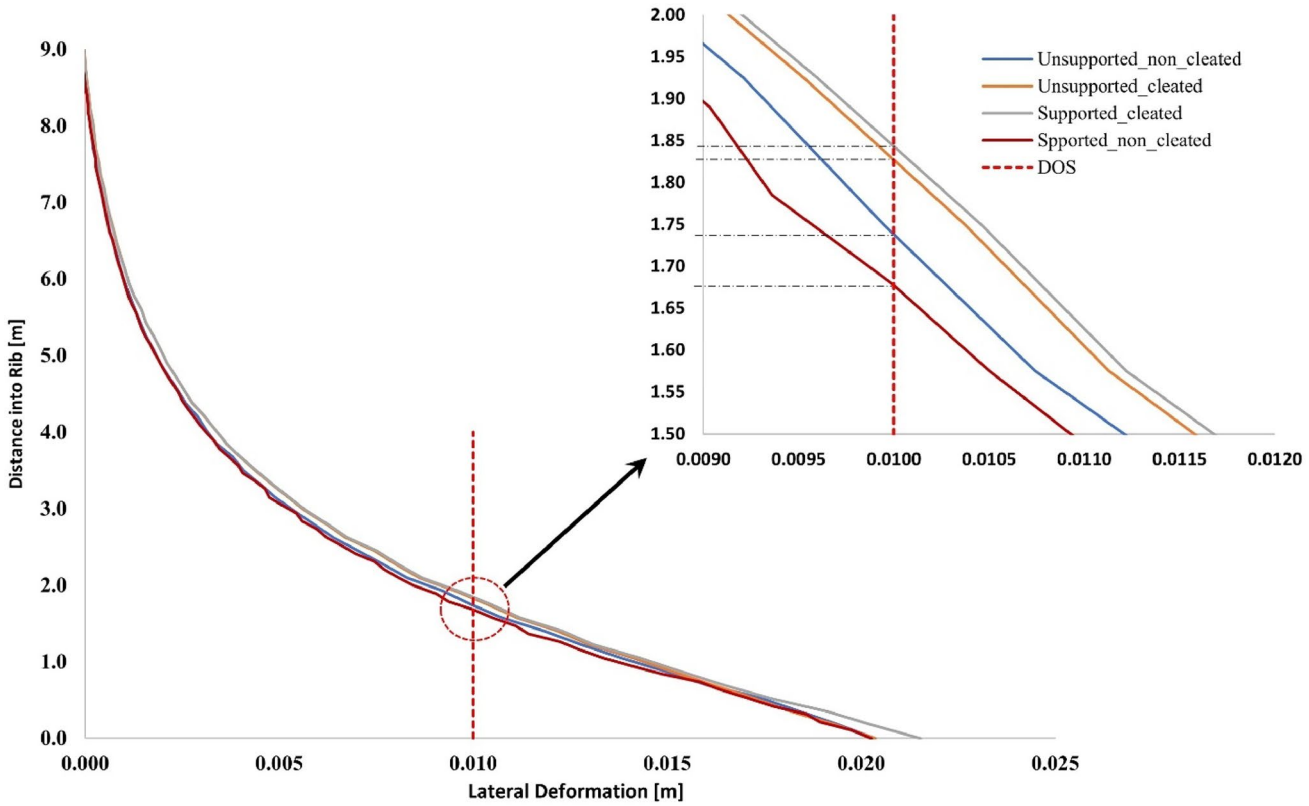

Fig. 11 Rib displacement response and DOS estimation for the four scenarios investigated in this study

rib is approximately 1.67 m and is the lowest, while the DOS for the cleated supported rib is almost the same as the cleated, unsupported rib at ~ 1.84 m. The support performance in the cleated rib is questionable when considering the DOS for the support and unsupported cases. The load transfer from coal to the rib bolts is extremely poor in this situation. The rib being full of structure (i.e., cleat) will cause blocks of coal to move independently of a stiff rock bolt and simply unravel around it.

4.5 Rib Factor of Safety Analysis

Dawson et al. (1999) demonstrated a failure state in a rock slope in which there is a sharp break in the unbalanced force when the strength reduction reaches a certain limiting value for an elastic perfectly-plastic model. The lateral displacement is another stability factor that could be used for such analysis, and it is apt for this research since the rib is a local part of the model being analyzed, unlike in Dawson's case where the slope was treated for its global stability. The smooth, well transitioned stability/failure curve obtained by Dawson's perfectly plastic model might be difficult to obtain in the BBM model because of the effect of block translations and rotations during failure. A global stability factor might not be suitable for a model where the interest is in the stability of a localized area. In view of this, lateral displacement is examined in this study with respect to the strength reduction process. In practice, mining engineers are interested in lateral movement to evaluate mine side-walls stability. Extensometers are usually installed to measure this motion. Nevertheless, block falls triggered by axial displacement is a strong possibility and also the two displacements are related in that it is the axial displacement that determines the magnitude of the lateral movement. Figure 12a presents the lateral displacement plots with increasing strength reduction factor for supported and unsupported cases of the rib BBM models. An average of three monitoring points located 20 cm into the rib was used to track the lateral displacement (Fig. 12b). It is important to ensure these points are not chosen close to the rib line because blocks near the rib line are prone to local failure and may result in estimation of extraneous displacement for this purpose. As observed in the near horizontal section of the plots, incrementing the SRF almost have the same effect on the lateral displacement for both the supported and unsupported rib models. The effect is clearer after the limiting FS for each case is reached: 1.49 for the non-cleated unsupported rib; 1.40 for the cleated unsupported rib; 1.80 for the supported non-cleated rib and 1.50 for the supported cleated models. These are indicated by the red markers in Fig. 12.

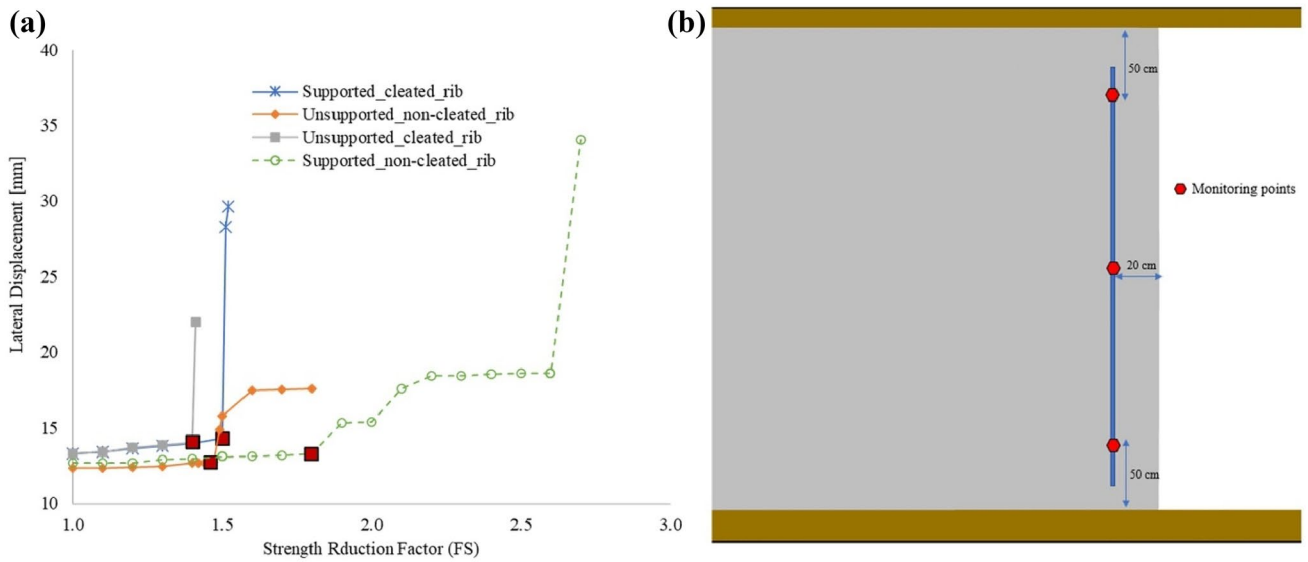

Fig. 12 Lateral displacement as a stability marker during the strength solution process (**a**). The three monitoring points and their locations with respect to the rib geometry are indicated in (**b**)

A stable rib will have displacement in the horizontal/flat section of the plot in Fig. 12a, while an unstable rib will have more displacement and, in this case, displacement after the elbow mark of the plots in Fig. 12a. An unstable rib will not become stable with continued cycling. When the cycling steps are increased after the rib displays instability, the rib will collapse as a result of intense fracture generation and propagation. Also, the models will never converge to a solution as the models become unstable. A sharp increase in displacement illustrates the transition point for a stable and unstable rib. A rapid fracture development, coalescence, and propagation in the model also helped in differentiating between a stable and unstable rib. There is a dominance of shear crack development in unstable models as previously developed tensile cracks begin to connect via shear as the rib fails.

5 Discussion and Prospects

This study examined the mechanics of rib stability control using numerical methods. It is impractical for mine operators to run numerical models to determine rib performance. A means of classifying or rating the rib failure mechanisms could be used as a foundation upon which rib control design methodology can be developed. The rib failure mechanisms identified in this study will help determine the type of rib support and infrastructure to be installed. The observations in this study provide a good starting point for developing a rating scale for the resultant failure based on dependent factors such as the overburden depth, stress environment, mining height, and coal strength. These factors can easily be measured in the mines. The BBM approach presented in this study suggests the rib behavior can be quantified. Quantifying the depth of softening, depth of fracture, total rib displacement, the dimensions of the failed blocks, the location of failure initiation in the rib, presents a great opportunity to develop a relationship between them and the measurable factors. Based on the results of this study, a classification system could suggest a different support system for the failures observed in the cleated and non-cleated ribs. For example, the large chunks of blocks observed in the non-cleated rib may need a high density of support with meshing. The failures observed in the cleated rib suggest a mesh or liner type support of sufficient coverage would be more suitable. Another important observation worthy of note is the fact that in the DOS estimation, it appears to be no sufficient confinement offered by the support type used in the cleated rib. Frith and Ditton (1993) observed a similar poor reinforcement performance in highly stressed and cleated seams and suggested that the load transfer from coal to the rib support is extremely poor under such conditions. This is mostly because the cleat causes the blocks to move independently of the stiff rib rock bolt and become loose around the support. A good load transfer requires coal mass conditions to exhibit a good level of competency and move en masse, as observed in the non-cleated rib. In a highly cleated/fractured coal mass, the potential to slip is very high, thus engineering very poor load transfer, and the bolts remain a passive component within this softened material (Frith & Ditton 1993). The fact that it is not practical for mines to employ numerical models at all times to determine

support requirements elicits the need for a simple tool based on easily measurable parameters that define rib performance. There are significant safety, productivity, and cost benefits to be gained by defining such a method. Such a prediction method could be very important in guiding ground control engineers and mine operators to plan and optimize the support requirements of their operations.

6 Conclusions

This study presented a gradual strength reduction process of the coal mass to determine the safety factor of the coal ribs. The method illustrated the progressive development of cracks in the rib of the pillar at each stage of the strength reduction process until failure. It should be noted that the accuracy of the solution greatly depends on the field evaluation of the strength parameters of the coal measured rocks. Fracture development in the rib is found to increase with a reduction in strength of the coal mass. Fracturing is less pronounced in the cleated rib compared with non-cleated coal rib. The cleated rib also has less deformation. The non-cleated rib will most likely produce a large slab of coal at failure, while the cleated rib will eject brittle granular coal. Based on this analysis, the depth of fracture needing reinforcement is about ~ 1.14 m for cleated and ~ 1.40 m for non-cleated. This value is based on the result that the stress relaxed/diminishes at this distance from the ribline; the rib fractured to this depth before failure, and the maximum deformation into the rib is recorded up to this depth.

The concept of rib instability is incorporated in the strength reduction method for this study and is demonstrated using lateral displacement/FS plots. These plots elicit the relationships between the limiting strength reduction factor and the lateral displacement to cause instability. The limiting value of the strength reduction factor is a good indicator of the factor of safety when the lateral displacement is considered. Because of the tendency for Voronoi blocks to rotate rather than translate laterally after failure, careful consideration is needed when selecting the monitoring points to compute the displacements. In this analysis, the marginal FS for the unsupported non-cleated, unsupported cleated, supported non-cleated, and supported cleated ribs were calculated to be 1.42, 1.30, 1.71, 1.44, respectively. These values agree approximately with results presented by other researchers for the same coal lithotype.

The support efficiency of the pillar is also evaluated in this study, and it is observed that support provides an improvement to the rib stability, as can be observed in the increased FS calculated. The supported models also demonstrated a confining effect in limiting the development of cracks in the rib. Lateral deformation and relaxation zones are also reduced with the introduction of rib supports. The rib with support failed at a much gradual pace when compared with unsupported ribs that failed violently. These findings underscored the BBM method to offer a promising approach to study the coal rib damage process and to recommend methods for support requirement prediction.

Acknowledgements The authors would like to acknowledge the support of the National Institute for Occupational Safety and Health (NIOSH) for their support in making this research possible.

References

Barton N, Shen B (2017) Risk of shear failure and extensional failure around over-stressed excavations in brittle rock. J Rock Mech Geotech Eng 9(2):210–225

Bigby DN, Cassie J (2003) Stability and support of sides of mine roadways. HSE Books

Cai M, Kaiser PK (2014) In-situ rock spalling strength near excavation boundaries. Rock Mech Rock Eng 47(2):659–675

Cala M, Flisiak J (2003) Complex geology slope stability analysis by shear strength reduction. FLAC and numerical modelling in geomechanics. AA Balkema Publishers, pp 99–102

Cheng YM, Lansivaara T, Wei WB (2007) Two-dimensional slope stability analysis by limit equilibrium and strength reduction methods. Comput Geotech 34(3):137–150

Christianson M, Board M, Rigby D (2006) UDEC simulation of triaxial testing of lithophysal tuff. The 41st US Symposium on Rock Mechanics (USRMS). American Rock Mechanics Association

British Coal (1990) Development of geotechnical design software for roadways and support systems. Final Report on ECSC Research Project No. 7220-AB818.

British Coal (1992) Design of roof bolted roadways. Final Report on ECSC Research Project No. 7220-AB827.

British Coal (1993) Strata measurement data analysis and presentation. Final Report on ECSC Research Project No. 7220-AB831.

Coggan J, Gao F, Stead D, Elmo D (2012) Numerical modelling of the effects of weak immediate roof lithology on coal mineroadway stability. Int J Coal Geol 90:100–109

Colwell MG (2006) A study of the mechanics of coal mine rib deformation and rib support as a basis for engineering design. University of Queensland

Colwell M, Mark C (2005) Analysis and design of rib support (ADRS) a rib support design methodology for Australian Collieries.

Dadashzadeh N (2020) Reliability of stress induced damage predictions in hard rocks with continuum and discontinuum numerical modelling approaches. (Doctoral dissertation).

Dawson EM, Roth WH, Drescher A (1999) Slope stability analysis by strength reduction. Geotechnique 49:835–840

Diederichs MS (2007a) The 2003 geotechnical colloquium: mechanistic interpretation and practical application of damage and spalling prediction criteria for deep tunnelling. Can Geotech J 44(9):1082–1116

Diederichs MS, Lato M, Hammah R, Quinn P (2007) Shear strength reduction approach for slope stability analyses. In Proceedings of the 1st Canada–US rock mechanics symposium. In: E Eberhardt, D Stead, T Morrison (eds) Vancouver.

Edelbro C (2009) Numerical modelling of observed fallouts in hard rock masses using an instantaneous cohesion-softening friction-hardening model. Tunn Undergr Space Technol 24(4):398–409

Esterhuizen GS (2014) Extending empirical evidence through numerical modelling in rock engineering design. J South Afr Inst Min Metall 114(10):755–764

Esterhuizen GS (1998) The effect of structural discontinuities on coal pillar strength as a basis for improving safety in the design of coal pillar systems. Safety in Mines Research Advisory Committee. http://hdl.handle.net/10204/1347

Esterhuizen GS (2012) A stability factor for supported mine entries based on numerical model analysis. In Proceedings of the 31st international conference on ground control in mining, (p. 25). West Virginia University.

Fabjan T, Ivars DM, Vukadin V (2015) Numerical simulation of intact rock behaviour via the continuum and Voronoi tessellation models: a sensitivity analysis. Acta Geotechnica Slovenica 12(2):5–23

Frith RC, Ditton S (1993) Monitoring report for geomechanics of rib failure and development of appropriate support technology. ACIRL Report EGE 3087/1.

Frith R, Reed G (2019) Limitations and potential design risks when applying empirically derived coal pillar strength equations to real-life mine stability problems. Int J Min Sci Technol 29(1):17–25

Gale WJ, Mark C, Oyler DC, Chen J (2004) Computer simulation of ground behaviour and rock bolt. 23rd international conference on ground control in mining, (pp. 27–34). Virginia.

Galvin J (2016) Ground engineering: principles and practices for underground coal mining. Springer

Galvin J (2006) Considerations associated with the application of the UNSW and other pillar design formulae. n Golden Rocks 2006, The 41st US Symposium on Rock Mechanics (USRMS). American Rock Mechanics Association.

Gao FQ, Stead D (2014) The application of a modified Voronoi logic to brittle fracture modelling at the laboratory and field scale. Internat J Rock Mech Min Sci 1:1–14

Gao F, Stead D, Kang H (2014) Simulation of roof shear failure in coal mine roadways using an innovative UDEC Trigon approach. Comput Geotech 61:33–41

Gao F (2013) Imulation of failure mechanisms around underground coal mine openings using discrete element modelling. Doctoral dissertation, Simon Fraser University.

Ghazvinian E, Diederichs MS, Quey R (2014) 3D random Voronoi grain-based models for simulation of brittle rock damage and fabric-guided micro-fracturing. J Rock Mech Geotech Eng 6(6):506–521

Giam SK, Donald IB (1988) Determination of critical slip surfaces for slopes via stress-strain calculations. Fifth Australia-New Zealand Conference on geomechanics: prediction versus performance; preprints of papers (p. 461). Institution of Engineers.

Griffiths DV, Lane PE (1999) Slope stability analysis by finite elements. Geotechnique 49(3):387–403

Hajiabdolmajid V, Kaiser PK, Martin CD (2002) Modelling brittle failure of rock. Int J Rock Mech Min Sci 39(6):731–741

Hebblewhite BB, Lin B, Galvin J, Walter R, Drew J (1998) Coal mine rib mechanics – an improved. In: international conference on geomechanics (pp. 403–412). NSW.

Heritage Y (2019) Mechanics of rib deformation—Observations and monitoring in Australian coal mines. Int J Min Sci Technol 29(1):119–129

Hijazo T, González De Vallejo LI (2012) In-situ stress amplification due to geological factors in tunnels: the case of Pajares tunnels, Spain. Eng Geol 137:13–20

Itasca Consulting Group (2019) User's manual version 5.0. Inc., Minneapolis.

Kalamaras GS, Bieniawski ZT (1993) A rock mass strength concept for coal seams. In Proc. 12th Conf. ground control in mining, (pp. 274–283). Morgantown, VA.

Kazerani T, Zhao J (2010) Micromechanical parameters in bonded particle method for modelling of brittle material failure. Int J Numer Anal Meth Geomech 34(18):1877–1895

Kim BH, Larson MK (2017) Evaluation of bumps-prone potential regarding the spatial characteristics of cleat in coal pillars under highly stressed ground conditions. In 51st US Rock Mechanics/Geomechanics Symposium. American Rock Mechanics Association.

Kirsch EG (1898) Die theorie der elastizität und die bedürfnisse der festigkeitslehre. Zeitschrift Des Vereines Deutscher Ingenieure 42:797–807

Krahn J (2003) The 2001 RM Hardy lecture: the limits of limit equilibrium analyses. Canadian Geotech J 40(3):643–660

Laubach SE, Marrett RA, Olson JE, Scott AR (1998) Characteristics and origins of coal cleat: a review. Int J Coal Geol 35(1–4):175–207

Li ZK, Liu H, Dai R, Su X (2005) Application of numerical analysis principles and key technology for high fidelity simulation to 3-D physical model tests for underground caverns. Tunn Undergr Space Technol 20(4):390–399

Lisjak A, Grasselli G (2014) A review of discrete modeling techniques for fracturing processes in discontinuous rock masses. J Rock Mech Geotech Eng 6(4):301–314

Liu H, Sang S, Xue J, Wang G, Xu H, Ren B, Liu S (2016) Characteristics of an in situ stress field and its control on coal fractures and coal permeability in the Gucheng block, southern Qinshui Basin, China. J Nat Gas Sci Eng 36:1130–1139

Lorig L, Varona P (2001) Practical slope-stability analysis using finite-difference codes. In: WA Hustrulid (eds) In Slope stability in surface mining (pp. 115–124). Society for mining, metallurgy and exploration, Inc.

Lorig LJ, Varona P (2013) Guidelines for numerical modelling of rock support for mines. In: YP Brady (Ed.), In proceedings of the seventh international symposium on ground support in mining and underground construction (pp. 81–105). Australian Centre for Geomechanics.

Lorig LJ, Cundall PA (1989) Modeling of reinforced concrete using the distinct element method. Fracture of concrete and rock. Springer

Martin CD (1997) Seventeenth Canadian Geotechnical Colloquium: the effect of cohesion loss and stress path on brittle rock strength. Can Geotech J 34(5):698–725

Martin CD, Chandler NA (1994) The progressive fracture of Lac du Bonnet granite. Internat J Rock Mech Mining Sci Geomech Abst 31(6):643–659

Mohamed MK, Murphy MM, Lawson EH, Klemetti T (2016) Analysis of the current rib support practices and techniques in US coal mines. Int J Min Sci Techno 26(1):77–87

Mohamed K, Rashed G, Radakovic-Guzina Z (2020a) Loading characteristics of mechanical rib bolts determined through testing and numerical modeling. Int J Min Sci Technol 30(1):17–24

Mohamed K, Van Dyke M, Rashed G, Morgan MS, Robert K (2021) Preliminary rib support requirements for solid coal ribs using a coal pillar rib rating (CPRR). Internat J Mining Sci Technol 31(1):15–22

Mohamed KM, Cheng Z, Rashed G (2019) Coal rib stability based on the strength reduction of the coal mass model. In 53rd US rock mechanics/geomechanics symposium. American Rock Mechanics Association.

Mohamed K, Kimutis R, Xue Y, Rasheed G (2020) Rib support optimization for a room-and-pillar mine. In proceedings of the 39th international conference on ground control in mining.

Mohamed K, Van Dyke M, Rashed G, Sears MM, Kimutis R (2020a) Preliminary rib support requirements for solid coal ribs using a coal pillar rib rating (CPRR). Internat J Mining Sci Technol.

MSHA (2018) Preliminary accident reports, fatality alerts and fatal investigation reports. US department of labor. Mine safety and health administration.

Nasehi MJ, Mortazavi A (2013) Effects of in-situ stress regime and intact rock strength parameters on the hydraulic fracturing. J Petrol Sci Eng 108:211–221

Naylor DJ (1982) Finite elements and slope stability. In Numerical methods in geomechanics 229–244.
Nie DN (2011) Experimental analysis of the post-failure behavior of coal and rock under laboratory compression tests. Graduate Theses, Dissertations, and Problem Reports.
Rashed G, Mohamed K, Kimutis R (2021) A coal rib monitoring study in a room-and-pillar retreat mine. Int J Min Sci Technol 31(1):127–135
Rusnak J (2017) Coal strength variation by lithotype for highvolatile a bituminous coal in the Central Appalachian Basin. In Proceedings of the 36th International Conference on Ground Control in Mining, (pp. 198–207). West Virginia University.
Saati V, Mortazavi A (2011) Numerical modelling of in situ stress calculation using borehole slotter test. Tunn Undergr Space Technol 26(1):172–178
Sainsbury DP (2008) Analysis of river bed cracking above longwall extraction panels in the Southern Coalfield of New South Wales, Australia. Proc. 1st Southern Hemisphere International Rock Mechanics Symp (pp. 325–338). Australian Centre for Geomechanics.
Sakurai S, Akutagawa K, Takeuchi K, Shinji M, Shimizu N (2003) Back analysis for tunnel engineering as a modern observational method. Tunn Undergr Space Technol 18(2–3):185–196
Salamon MD (1970) Stability, instability and the design of pillar workings. Int J Rock Mech Min Sci 7:613–631
Salamon MG, Munro AH (1967) A study of the strength of coal pillars. J South Afr Inst Min Metall 68(2):55–67
Salamon MD (1974) Rock mechanics of underground excavations. In Advances in rock mechanics. Proceedings 3rd Congr Int Soc Rock Mech (pp. 951–1099). Denver: Nat. Acad. Sci.
Sears MM, Rusnak J, Van Dyke M, Rashed G, Mohamed K, Sloan M (2018) Coal rib response during bench mining: a case study. Int J Min Sci Technol 28(1):107–113
Shepherd J (2002) Assessment of rib instability hazards for strata management systems. In: Aziz N (ed) University of Wollongong research onlinecoal operators' conference. University of Wollongong & the Australasian Institute of Mining andMetallurgy, pp 122–125
Singh M, Seshagiri RK (2005) Empirical methods to estimate the strength of jointed rock masses. J Geophys Eng 77:127–137
Sinha S, Walton G (2021) Investigation of pillar damage mechanisms and rock-support interaction using Bonded Block Models. Internat J Rock Mech Mining Sci 138.
Sinha S, Walton G (2020) A study on Bonded Block Model (BBM) complexity for simulation of laboratory-scale stress-strain behavior in granitic rocks. Comput Geotech 118:103363
Smith WC (1992) Rib stability: practical considerations to optimize rib design (Vol. 9323). US Department of the Interior, Bureau of Mines.
Sunkpal M, Alebayat M, Taghi S (2020) Coal rib geomechanics: a numerical approach for the analysis of rib stability in underground coal mines. 54th US Rock mechanics/geomechanics symposium. American Rock Mechanics Association.
Tulu IB, Esterhuizen GS, Klemetti T, Murphy MM, Sumner J, Sloan M (2016) A case study of multi-seam coal mine entry stability analysis with strength reduction method. Int J Min Sci Technol 26(2):193–198
Ugai K, Leshchinsky DO (1995) Three-dimensional limit equilibrium and finite element analyses: a comparison of results. Soils Found 35(4):1–7
Vardar O, Zhang C, Canbulat I, Hebblewhite B (2019) Numerical modelling of strength and energy release characteristics of pillar-scale coal mass. J Rock Mech Geotech Eng 11(5):935–943
Walton G, Diederichs MS (2015) A mine shaft case study on the accurate prediction of yield and displacements in stressed ground using lab-derived material properties. Tunn Undergr Space Technol 49:98–113
Walton G, Diederichs M, Punkkinen A, Whitmore J (2016) Back analysis of a pillar monitoring experiment at 2.4 km depth in the Sudbury Basin, Canada. Int J Rock Mech Min Sci 85:33–51
Wilson AH (1983) The stability of underground workings in the soft rocks of the Coal Measures. Int J Min Eng 1(2):91–187
Yaméogo ST, Corthésy R, Leite MH (2013) Influence of rock failure and damage on in situ stress measurements in brittle rock. Int J Rock Mech Min Sci 61:118–129
Zhang L (1997) Einstein HH (2004) Using RQD to estimate the deformation modulus of rock masses. Internat J Rock Mech Mining Sci 41(2):337–341
Zhang C, Mitra R, Oh J, Canbulat J, Hebblewhite B (2018) Numerical analysis on mining-induced fracture development around river valleys. Int J Min Reclam Environ 32(7):463–485
Zheng H, Sun G, Liu D (2009) A practical procedure for searching critical slip surfaces of slopes based on the strength reduction technique. Comput Geotech 36(1–2):1–5
Zheng YR, Zhao SY, Song YK (2005) Advance of study on the strength reduction finite element method. J Log Eng Univ
Zhu WS, Sui B, Li XJ, Li SC, Wang WT (2008) A methodology for studying the high wall displacement of large scale underground cavern complexes and it's applications. Tunn Undergr Space Technol 23(6):651–664
Zhu WS, Zhang QB, Hong-Hu Z, Yong L, Yin JH, Li SC, Zhang L (2010) Large-scale geomechanical model testing of an underground cavern group in a true three-dimensional (3-D) stress state. Can Geotech J 47(9):935–946
Zhu DF, Tu F, Ma HS, Zhang XW (2017) A 3D Voronoi and subdivision model for calibration of rock properties. Model Simul Mater Sci Eng 25(8):085005
Zhu D, Wu Y, Liu Z, Dong X, Yu J (2020) Failure mechanism and safety control strategy for laminated roof of. Engineering Failure Analysis 111.
Zienkiewicz OC, Humpheson C, Lewis RW (1975) Associated and non-associated visco-plasticity and plasticity in soil mechanics. Geotechnique 25(4):671–689
Zipf K (2006) Numerical modeling procedures for practical coal mine design. The 41st US Symposium on Rock Mechanics (USRMS). American Rock Mechanics Association